JOURNAL OF MATERIALS SCIENCE 37 (2002) 523–530

Fail-safe light transmitting SiC fiber-reinforced spinel matrix optomechanical composite

A. F. DERICIOGLU, Y. KAGAWA*
Institute of Industrial Science, The University of Tokyo, 4-6-1, Komaba, Meguro-ku, Tokyo 153, Japan
E-mail: kagawa@iis.u-tokyo.ac.jp

A light transmitting "Optomechanical Composite" was fabricated by incorporating SiC (SCS-6) fibers into optically transparent $MgAl_2O_4$ ceramics. The fibers were aligned unidirectionally in the matrix with a spacing of 1 to 4 mm to allow light transmittance between the fibers: resulting fiber volume content was from 0.75 to 0.19 vol%. The total and in-line light transmittance of the matrix and the composite was measured in the visible/near-IR wavelength region. The light transmittance of the composite was found to be decreasing with increasing fiber volume fraction, however, even the composite with the highest fiber volume fraction has a light transmittance of 25–50% in the visible wavelength region. Although the optical transparency of the matrix becomes slightly lower by the incorporation of the opaque fibers, its catastrophic failure is prevented by the bridging effect of the intact fibers, introducing the fail-safe nature to the brittle ceramic material. To obtain this fail-safe mechanism, the minimum fiber volume fraction was ~0.37 vol% in the present material system. © *2002 Kluwer Academic Publishers*

1. Introduction

Several oxide and non-oxide ceramic materials have good optical transparency in the visible/infrared wavelength regions. These transparent ceramics are expected to be used in various applications such as armor windows, domes, windshields and monitoring windows etc. Among these transparent ceramics, magnesium aluminate spinel ($MgAl_2O_4$) has received considerable attention and has been studied extensively [1–6] because of the good combination of its optical and mechanical properties both at ambient and elevated temperatures. Currently, $MgAl_2O_4$ is expected to serve as a high temperature window material because of its isotropic optical properties due to the spinel structure, high temperature strength and chemical inertness to alkalis and oxidation [7]. The major drawback of this application arises from its low fracture toughness, which leads to low reliability of the material under service conditions.

Recently, a composite termed as "Optomechanical Composite" has been developed [8] and applied to glass, glass-ceramic materials and polymers in order to reach an optimum condition of both improved mechanical and optical properties [9–16]. The major problem of such composites is the difficulty in achieving interfacial requirements that lead to an improvement in mechanical and optical properties simultaneously. In addition, usually the dimension of the reinforcing second phase is an order of ten-micrometer resulting in a large amount of fiber-matrix interfacial area, and thus it is difficult to reduce the total amount of light scattering occurring at the interface by the incorporation of the second phase. To prevent light scattering, the refractive index difference between the constituents should be as small as possible [8, 11]. However, that condition is difficult to achieve in ceramic fiber-reinforced ceramic matrix optomechanical composites because of the limitations of available materials with suitable physical properties that fulfill the interfacial requirements for improved optical and mechanical properties.

The present study has focused on improving the fracture resistance of transparent ceramics by the incorporation of ceramic fibers without loosing the optical transparency of the matrix material. Here, unlike the previous approach used for glass or polymer matrix optomechanical composites, a newly proposed concept of "Optical Window" is applied to the continuous SiC fiber-reinforced $MgAl_2O_4$ (magnesium aluminate spinel) matrix composites. In this approach the amount of fiber-matrix interfaces is minimized by the regular alignment of the fibers in a mesh like structure, and a weak interfacial bonding is maintained for improved mechanical properties. With the new concept, the refractive index mismatch limitation is eliminated and light transmission of the composite is obtained through the use of transparent matrix regions surrounded by the incorporated fibers. Consequently, it is aimed that transparent ceramics including $MgAl_2O_4$ could be made reliable enough for applications requiring high optical transparency and fracture resistance, simultaneously, hence resulting in an increase in their areas of use.

*Author to whom all correspondence should be addressed.

TABLE I Properties of the fiber and the matrix

	Young's modulus E(GPa)	Strength (MPa)	Fracture toughness K_{Ic} (MPa$\sqrt{m}$)	Poisson's ratio (ν)	Coefficient of thermal expansion $\alpha \times 10^{-6}$ (K^{-1})
SiC fiber (SCS-6)[a]	406	3720 (Tensile)	–	0.15	5.00 (longitudinal) 2.63 (transverse)
$MgAl_2O_4$	248–270	~420[b]	1.4–1.7[c]	0.26	7.9

[a]Textron®.
[b]Measured by three-point bending test (except the strength and the fracture toughness, other properties of the matrix belong to the stoichiometric $MgAl_2O_4$).
[c]Fracture toughness of $MgAl_2O_4$ is the measured value obtained through the "Compact Tension Specimen."

2. Experimental procedure

2.1. Fabrication of composite

A $MgAl_2O_4$ powder was prepared from commercially available high purity MgO (purity 99.98 wt%, 1000A, Ube Chemicals Co. Ltd., Ube, Japan) and Al_2O_3 (purity 99.99 wt%, TM-DAR, Taimei Chemicals Co. Ltd., Nagano, Japan) powders having average particle sizes less than 0.12 and 0.15 μm, respectively. In a preliminary study, the authors have investigated the fabrication of optically transparent monolithic $MgAl_2O_4$ for different starting powder compositions applying various combinations of processing conditions and determined that the optimum starting powder composition of the matrix should be 1 to 1.5 in terms of MgO and Al_2O_3 molar ratios, respectively [17].

A continuous SiC fiber (SCS-6, Textron Inc., Lowell, MA, USA) was unidirectionally incorporated into the $MgAl_2O_4$. The SiC fiber has an outer diameter of ~140 μm with a 40 μm diameter carbon core and a ~3.6 μm thick outermost β-SiC particle-dispersed carbon coating layer [18]. The typical properties of the $MgAl_2O_4$ matrix and the SiC fiber are listed in Table I [19–21].

The starting matrix powder was wet ball-milled in ethyl alcohol for 24 h. The wet powder mixture was dried in an oven at 373 K for 5 h and the resulting agglomerates were sieved below 500 μm particle size. The fiber preform was prepared by a hand lay-up method. The SiC fiber was aligned unidirectionally with a uniform spacing, $d_s = 1, 2, 4$ mm, which corresponds to a fiber volume fraction, V_f, of 0.75, 0.37 and 0.19 vol%, respectively. Here, fiber volume fraction was defined as V_f = (Fiber volume/Total composite volume) × 100. The fiber preforms were embedded into the $MgAl_2O_4$ matrix powder in the hot pressing mould. Hot pressing was conducted at 1673 K in a vacuum of 10^{-2} Pa for 1 h under a pressure of 50 MPa. The hot-pressed composites were hot isostatically pressed (HIP) to achieve full densification. HIPing was done at 2173 K in argon for 1 h under a pressure of 189 MPa. The fabrication flow chart of the composites including the powder preparation stage is shown in Fig. 1.

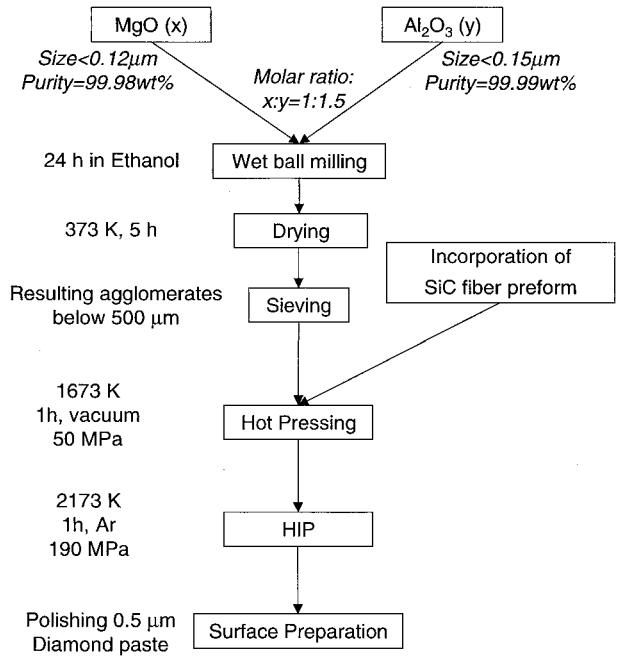

Figure 1 Fabrication process of the composites including the powder preparation stages.

2.2. Characterization

The microstructure of the composites was examined using a conventional optical microscope (BUH, Olympus Co. Ltd., Tokyo, Japan) under reflective light and cross-polarized transmission light. Scanning electron microscopy was also carried out using a conventional SEM (JSM-5310LV, Jeol Ltd., Tokyo). Before microstructural examination the polished specimens were thermally etched in ambient air at 1473 K for 1 h in order to reveal the microstructure.

The crystalline structure of the $MgAl_2O_4$ was determined by an X-ray diffraction method using a Mo target with a conventional X-ray diffractometer (RINT2500, Rigaku Corporation, Tokyo). The polished surfaces of monolithic $MgAl_2O_4$ perpendicular to the hot-pressing direction were analyzed.

2.3. Light transmittance measurement

As fabricated composites were cut to appropriate size and their surfaces were polished with a standard metallurgical process to obtain flat and parallel surfaces for the light transmittance measurements. The measurements were done at a wavelength range from 250 to 2000 nm using a transmission optical spectrometer (Jasco V-550 type, Nihon Bunko Corp., Tokyo) under a controlled temperature of 298 K. The resolution of the equipment in the measured wavelength range was less than 2 nm. The total and in-line transmission spectra of the composites were obtained in the direction perpendicular to the fiber axis using 2.0 ± 0.02 mm thick samples. The total transmission spectra were obtained by detecting both the specularly and diffusely transmitted light through the integrating sphere attachment (ISN-470,

Nihon Bunko Corp., Tokyo) of the spectrometer. On the contrary, the in-line transmission spectra were obtained by detecting only the specularly transmitted portion of the light through 3 mm diameter slits attached on both surfaces of the specimen perpendicular to the light propagation direction. During the light transmission measurements specimens were rotated by 90 degrees after each measurement in order to eliminate the polarization effects, and the average of the four obtained spectra was used for the analysis.

2.4. Mechanical testing

A compact tension (CT) specimen with dimensions of 31 by 30 by 2 mm was prepared. The notch depth, a, to width, W, ratio was $a/W \sim 0.53$. A chevron type starter notch with a tip angle of 60 degrees was used, and the length difference between its two side edges was less than 0.05 mm. The notch, whose width was $\sim$200 μm, was introduced perpendicular to the fiber axis direction of the CT specimen. A schematic drawing of the CT specimen with its dimensions and the fiber axis direction is shown in Fig. 2. The CT specimens were tested with a pin-loading system using a screw-driven type testing machine (AG-500E, Shimadzu Corp., Kyoto, Japan; maximum loading capacity: 5 kN). Tests were conducted at a fully controlled temperature of 298 K with a cross-head displacement rate of 1 and 10 μm/min. During the test, the load versus time relation was continuously recorded by a digital memory scope (ORM 1200, Yokogawa Corp., Tokyo) at a sampling rate of 20 ms. The crack growth behavior was monitored by a CCD camera and the image was continuously stored to a VTR system at a frame rate of 1/30 s. The crack length at the onset of unstable crack growth was measured from the VTR recording. The test was interrupted when the matrix crack proceeded unstably. The fracture toughness, K_{Ic}, of the specimens was calculated by [22],

$$K_{Ic} = \frac{P_c}{BW^{1/2}} \times \frac{\left(2+\frac{a}{W}\right)\left[0.886+4.64\frac{a}{W}-13.32\left(\frac{a}{W}\right)^2+14.72\left(\frac{a}{W}\right)^3-5.6\left(\frac{a}{W}\right)^4\right]}{\left(1-\frac{a}{W}\right)^{3/2}}. \quad (1)$$

Here, P_c is the load at the onset of unstable crack growth, B and W are the thickness and the width of the CT specimen, respectively, and a is the notch length.

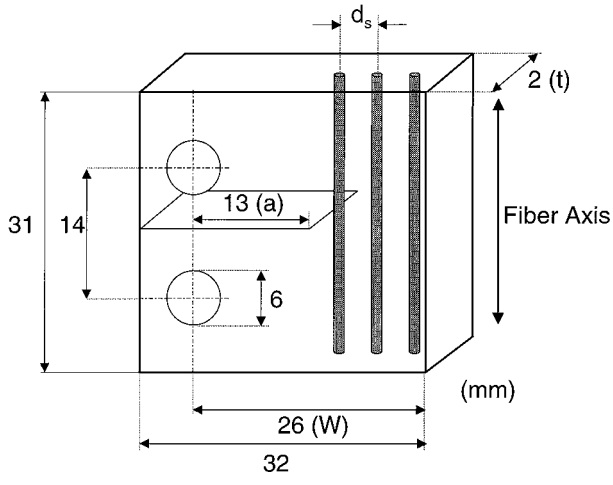

Figure 2 Schematic drawing of the CT specimen showing its dimensions and the fiber axis direction.

3. Results and discussion

3.1. Characterization

The appearance of as-fabricated monolithic $MgAl_2O_4$ and composites with two different fiber spacings, $d_s = 1$ and 2 mm, are shown in Fig. 3. The photograph was taken after the preparation of the CT specimens. The SiC fibers are clearly seen in the composites as thin black lines, however, the underlying letters are clearly legible through the matrix region of the composites. This appearance seems natural because the matrix region of the composites has light transmittance like a monolithic matrix material.

SEM observation of the thermally-etched surfaces reveals a homogeneous grain size distribution (Fig. 4) of the $MgAl_2O_4$ matrix with an average grain size of $\sim$15 μm. Here, the grain size is obtained using a quantitative metallographic method by counting the intersection points that the drawn test lines make with the grain boundary network on the obtained micrographs [23]. The average grain size is different from the results obtained in a previous study by the present authors [24], in which the average grain size of a $MgAl_2O_4$ ranged from 140 to 650 μm for different processing conditions used. Additionally, the previous $MgAl_2O_4$ contains a considerable amount of microcracking along its grain boundaries. Although both of these studies use similar processing conditions, the starting powder compositions are different, i.e. while the present study uses a MgO to Al_2O_3 molar ratio of 1 : 1.5, the previous study uses a ratio of 1 : 1. The difference in the microstructures of both cases is thought to result from the difference of chemical composition, further investigation is needed to understand the effect of chemical composition on the microstructure, however.

XRD analysis of the matrix phase in the composites reveals that their matrix consists of a single phase magnesium aluminate spinel. The X-ray diffraction pattern obtained from the composite matches with the pattern of a standard synthetic $MgAl_2O_4$ [25] with a slight shift in the positions of their peaks. This shift is due to the difference in the chemical composition of the

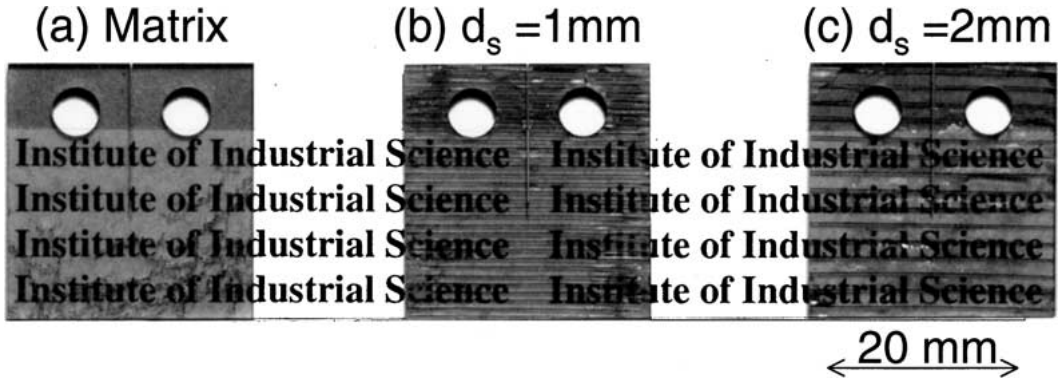

Figure 3 Appearance of the fabricated monolithic matrix and the composites with two different fiber spacing, d_s.

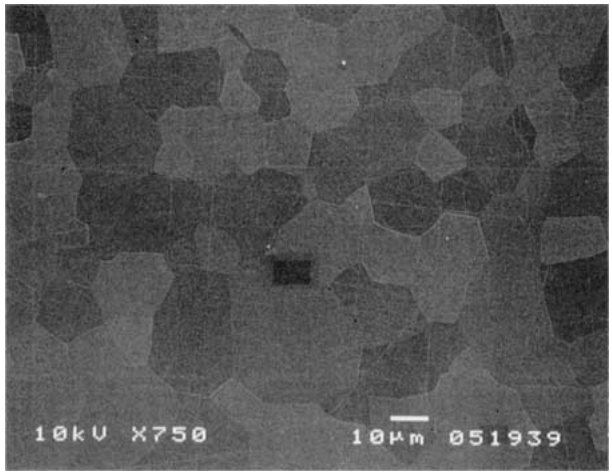

Figure 4 SEM micrograph showing the microstructure of the $MgAl_2O_4$ matrix.

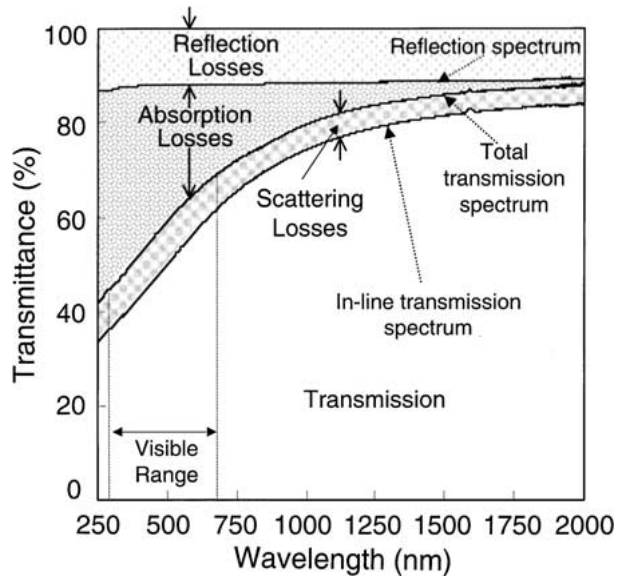

Figure 5 Total, in-line and reflection spectra of the monolithic $MgAl_2O_4$ matrix.

fabricated $MgAl_2O_4$ and the standard one. Hereafter the matrix of the fabricated composites is termed as monolithic $MgAl_2O_4$. It should be noted that the chemical composition of the present matrix is different from the stoichiometric $MgAl_2O_4$ because of its higher Al_2O_3 content, which causes the slight shift of the peaks in the pattern.

3.2. Light transmittance

The measured light transmittance of the monolithic $MgAl_2O_4$ is in good accordance with its appearance (Fig. 3a). The measured total and in-line transmission spectra of the monolithic $MgAl_2O_4$ in the visible/near-IR wavelength region are shown in Fig. 5 together with its measured light reflection spectrum. As can be seen from Fig. 5, the reflection spectrum is nearly constant at a value of ∼90%, suggesting that nearly 10% of the incoming light is reflected at the outer and inner surfaces of the specimens. The total transmission spectrum (containing both specular and diffuse transmission) of the monolithic $MgAl_2O_4$ is nearly constant at a value of ∼80% in a wavelength range from 2000 to 1625 nm, and it starts to decrease below ∼1625 nm because of absorption losses [26].

The in-line transmission spectrum of the monolithic $MgAl_2O_4$ is slightly lower than its total transmission spectrum. However, the difference of transmittance between these two spectra is nearly constant at a value of ∼5% in the measured wavelength range. This difference shows that the amount of scattering or diffuse transmission of light in monolithic $MgAl_2O_4$ is considerably lower. As a result of both facts, the minimum value of the total transmission spectrum being above 25% and the amount of scattered light being ∼5% throughout the visible wavelength range, it is clear that the fabricated $MgAl_2O_4$ ceramics have good optical transparency.

The total light transmission spectra of the monolithic $MgAl_2O_4$ and the fabricated composites for different fiber spacing (fiber volume fractions) are shown in Fig. 6. The figure demonstrates that the light transmission of the composite decreases with decreasing fiber spacing, d_s. This is, in fact, not an unexpected result since the SiC fiber is an opaque material in the measured wavelength range. The decrease in the light transmittance of the SiC fiber-reinforced $MgAl_2O_4$ matrix composites is obviously attributed to the increasing shadow area of the fibers.

The shadow area, S_s, of the opaque SiC fibers is defined as the shadow area originated by the addition of the fibers. The matrix region of the composite contributing to the light transmission is defined as the window area, S_w (Fig. 7). The total light transmittance of the monolithic matrix is given by,

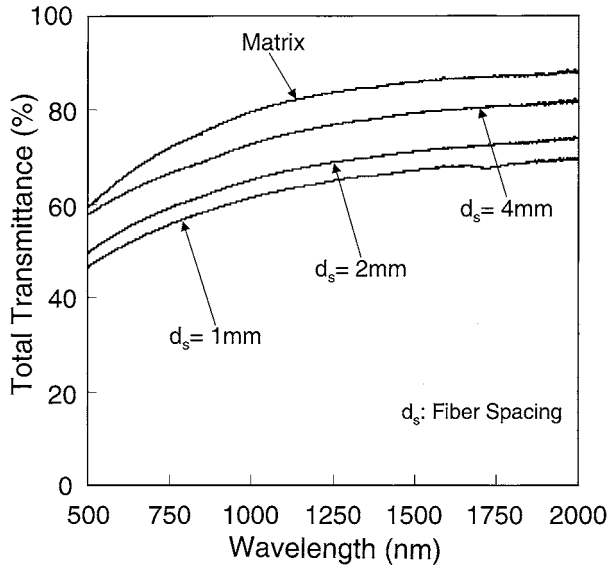

Figure 6 Total transmission spectra of the monolithic $MgAl_2O_4$ matrix and the composites with changing fiber spacing, d_s.

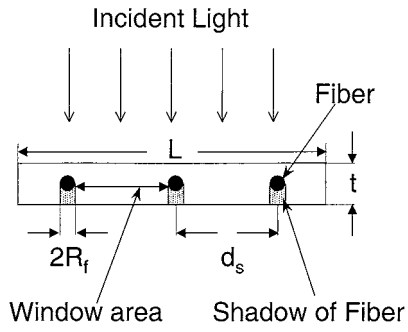

Figure 7 Schematic drawing of the top view of the composite and definition of the parameters used for the calculations.

$$T_m \approx (1 - R)^2 \exp(-\alpha_{abs} t) \tag{2}$$

where R is the reflectance and α_{abs} is the absorption coefficient of the material, and t is the thickness of the specimen. The decrease in the light transmission of the monolithic matrix caused by the incorporation of the fibers can be explained simply by the ratio of the total shadow area, S_s, to the total composite area, S_c. In other words, the light transmission of the composite is only achieved by a matrix area that is given by the ratio of the total window area, S_w, to the total composite area, S_c. The light transmittance of the present optomechanical composite, T_c^*, is given by,

$$T_c^* = \frac{S_w}{S_c} T_m = \left(1 - \frac{S_s}{S_c}\right) T_m. \tag{3}$$

The surface area of the composite per unit height of the specimen perpendicular to the light propagation direction is given by,

$$S_c = d_s N_f \tag{4}$$

where d_s is the fiber spacing and N_f is the number of fibers per unit area of the composite. For the fibers located nearest to the edge of the composite the first fiber spacing is taken as $d_s/2$. Similarly, the shadow area of the fibers per unit height of the specimen is given by,

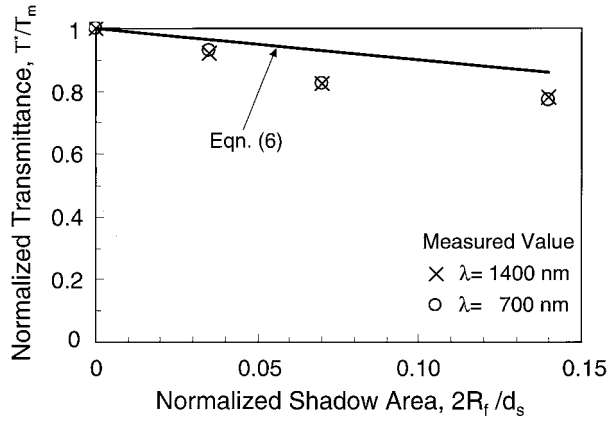

Figure 8 Normalized total transmittance versus $2R_f/d_s$ showing the decrease in light transmittance of the composite with increasing shadow area.

$$S_s = 2R_f N_f \tag{5}$$

where R_f is the fiber radius. Substituting Equations 4 and 5 into Equation 3, the normalized light transmittance of the composite, T_c^*/T_m, is,

$$\frac{T_c^*}{T_m} = \left(1 - \frac{2R_f}{d_s}\right). \tag{6}$$

The measured normalized light transmittance of the composites, T_c/T_m, for two different wavelengths is plotted against $2R_f/d_s$ together with the estimation of T_c^*/T_m (Equation 6). As can be seen from Fig. 8, the light transmittance of the composite decreases with increasing $2R_f/d_s$, suggesting that the light transmittance of the composite is predicted by the shadow area of the fibers. Although experimental values follow the trends of the estimation of Equation 6, they show slightly lower values compared to the estimation, which is probably due to the existence of microcracking near fibers (Fig. 9) causing scattering of light out of the detection area.

For the present case, it should be pointed out that although the amount of transmitted light decreases with decreasing fiber spacing, it does not drop below 25% in the visible wavelength region (350–700 nm) even for the composite with the shortest fiber to fiber separation distance. Consequently, it can be said that despite the decrease in the light transmission of the $MgAl_2O_4$ with the incorporation of fibers, the composite material has considerable optical transparency due to the presence of the window area of the $MgAl_2O_4$.

3.3. Characteristic mechanical properties

A typical example of a load-displacement curve of the CT specimen for the monolithic $MgAl_2O_4$ and the composite with $d_s = 1$ mm ($V_f = 0.75$ vol%) is shown in Fig. 10. The load increases linearly up to a maximum (P_c) without noticeable subcritical crack growth from a notch root. At the maximum, unstable crack growth

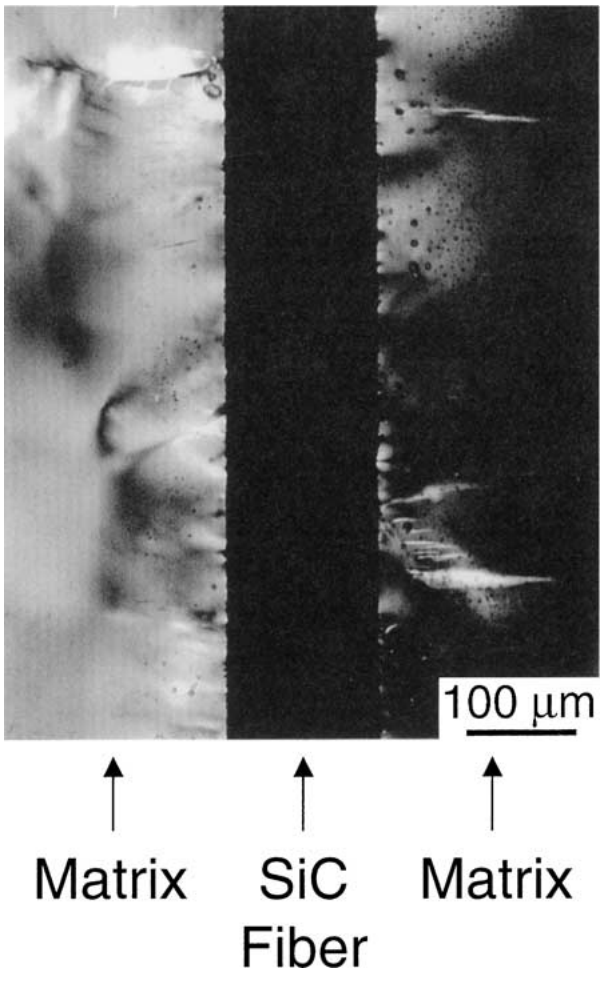

Figure 9 Cross-polarized transmission light optical micrograph showing the existence of microcracking in the $MgAl_2O_4$ matrix at the fiber-matrix interface.

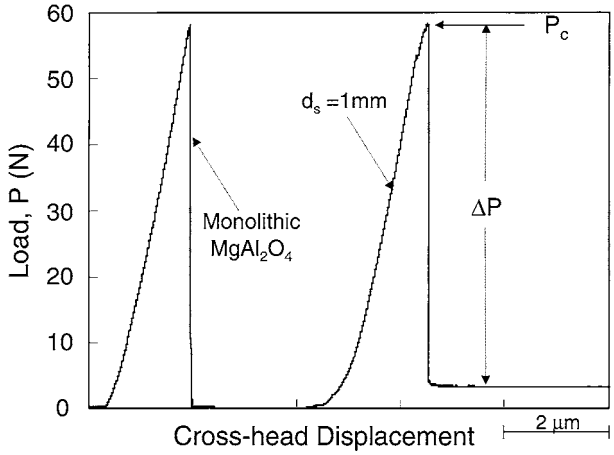

Figure 10 Typical load versus cross-head displacement curve of the CT specimen belonging to the monolithic $MgAl_2O_4$ and the composite with $d_s = 1$ mm.

occurs from the notch tip for both of the specimens. Just after the unstable crack growth the load decreases abruptly by an amount ΔP, however, it does not drop to zero for the composite since the intact fibers bridge the matrix crack. Fig. 11 shows the evidence of the operation of post matrix fracture fiber bridging for the composites with fiber spacing of 1 and 2 mm. The sudden load drop at the maximum originates from the matrix cracking and therefore the load drop, ΔP, corresponds to the load carried by a ligament area just before unstable crack growth.

The fracture toughness, K_{Ic}, of the monolithic $MgAl_2O_4$ and composites is shown in Fig. 12 as a function of fiber to fiber spacing, d_s. Although the measured values range from 1.65 to 1.80 MPa$\sqrt{\text{m}}$, the fracture toughness of the composite seems to be nearly constant independent of the fiber spacing. It seems natural since the fiber to fiber spacing is an order of millimeter and this length is much longer than the subcritical crack growth length from notch tip before unstable crack growth. As a result, a fiber bridging mechanism cannot operate before unstable crack propagation. The fracture toughness of the composite, K_{Ic}^c, is given by [27, 28],

$$K_{Ic}^c \cong \left(\frac{E_c}{E_m}\right) K_{Ic}^m + \Delta K_I^T \tag{9}$$

where K_{Ic}^m is the fracture toughness of the monolithic matrix, Δk_I^T is the effect of the thermally induced axial stress in the matrix on the fracture toughness of the composite, E_m is the Young's modulus of the matrix, and E_c is the longitudinal Young's modulus of the composite. ΔK_I^T is directly proportional to the longitudinal thermally induced stress in the matrix, $\Delta\sigma_m^T$, which is given by [27]

$$\Delta\sigma_m^T = \frac{\lambda_2}{\lambda_1}\left(\frac{E_f}{E_c}\right)\frac{f\left(\alpha_f^L - \alpha_m\right)\Delta T E_m}{(1-\nu_m)} \tag{10}$$

where E_f is the Young's modulus of the fiber, f is the fiber content ($V_f/100$), α_f^L and α_m are the thermal expansion coefficient of the fiber in the longitudinal direction and the matrix, respectively, ΔT is the temperature range over which residual stresses develop, and ν_m is the Poisson's ratio of the matrix. Additionally, λ_1 and λ_2 are functions of E_f, E_c, f and the Poisson's ratios of fiber and the matrix [29]. In the case of SiC fiber-reinforced $MgAl_2O_4$ matrix composites, thermal axial tensile stress develops in the matrix during the cooling of the composites after processing. This tensile stress in the matrix contributes to the decrease in the fracture toughness of the composite. However, in the present study ΔK_I^T is negligible since $\Delta\sigma_m^T \sim 0$ due to the low fiber content ($f \sim 0$). Additionally, longitudinal Young's modulus of the composite ($E_c \approx fE_f + (1-f)E_m$) is nearly the same as that of the matrix because of $f \sim 0$ and $E_f \approx E_m$. Under these conditions, Equation 9 reduces to

$$K_{Ic}^c \approx K_{Ic}^m. \tag{11}$$

This indicates that the toughness of the present composite is nearly the same as that of the monolithic $MgAl_2O_4$ matrix.

Although the toughness of the monolithic $MgAl_2O_4$ could not be improved, a fail-safe mechanism is introduced into the matrix by the incorporation of fibers that resulted from the load carrying capacity of the intact ones after the total fracture of the matrix. In addition, the light transmittance of the monolithic $MgAl_2O_4$ is

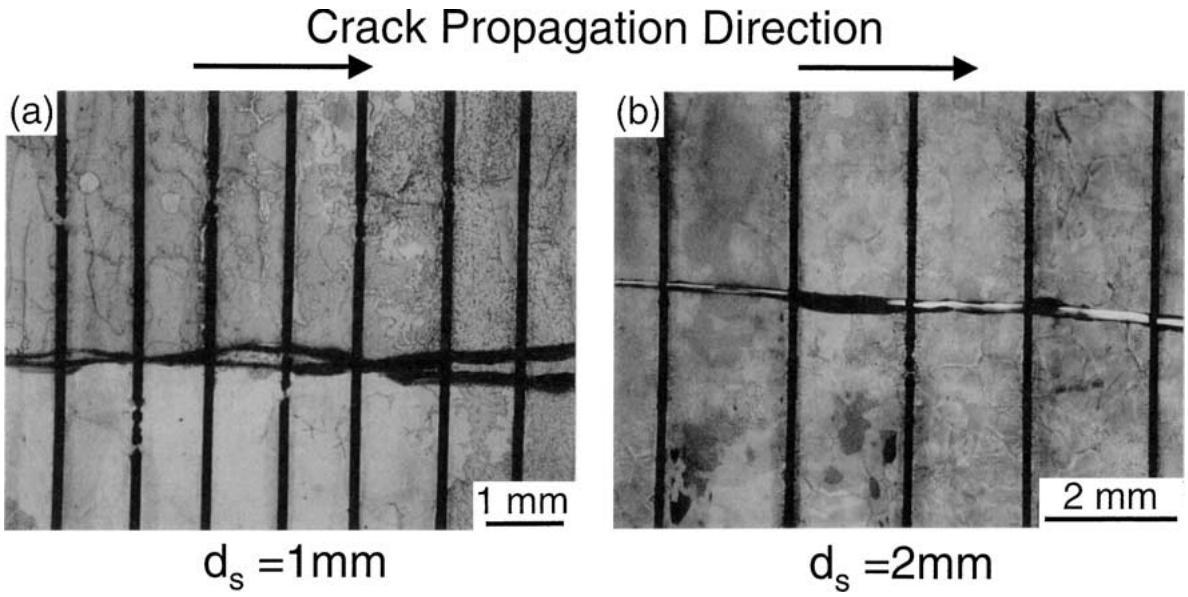

Figure 11 Optical micrographs of already tested CT specimens with (a) $d_s = 1$ mm and (b) $d_s = 2$ mm showing the matrix crack bridged by intact fibers.

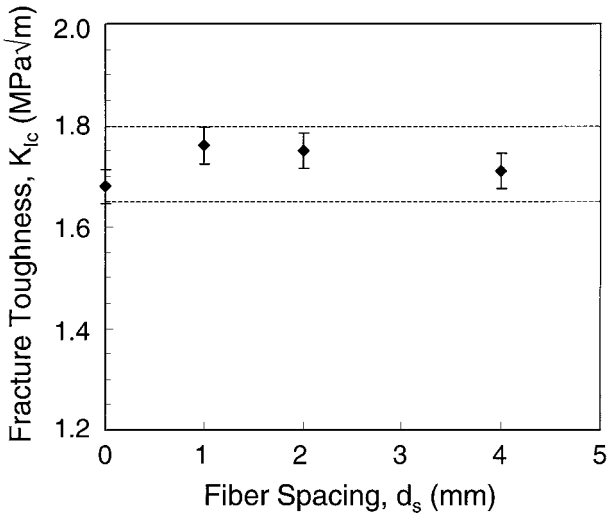

Figure 12 Plots of fracture toughness, K_{Ic}, of the monolithic $MgAl_2O_4$ and the composites versus fiber spacing, d_s.

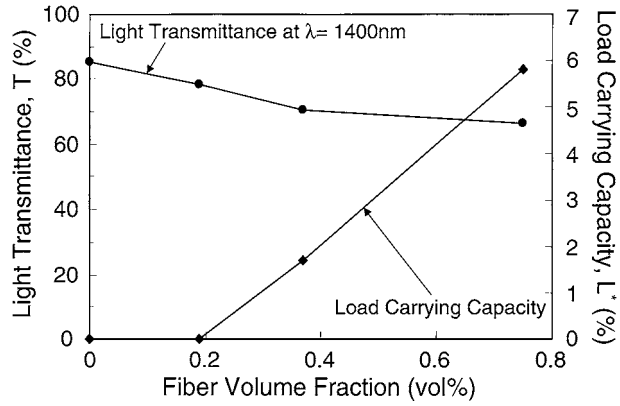

Figure 13 Fiber content dependence of the light transmittance, T, and the load carrying capacity, L^*, of the optomechanical composite.

mainly preserved through the window area of the composite despite the presence of the opaque SiC fiber. At that point it should be noted that the improvement of the mechanical and optical properties of the fabricated optomechanical composite depends inversely on the fiber volume fraction, i.e. increasing fiber volume fraction improves fail-safe capacity whereas the light transmitting capacity vice versa. This behavior can be shown by a plot in which light transmittance, T, and load carrying capacity, L^*, of the composite are given as a function of fiber volume fraction (Fig. 13). Here, the load carrying capacity, L^*, is defined as $(P_c - \Delta P)/P_c$ that gives the fraction of the load carried by the fibers following the unstable crack growth in the matrix to the maximum load reached. From Fig. 13 it is clear that the light transmittance of the composite decreases with increasing fiber volume fraction because of the increasing fiber shadow area. On the other hand, the load carrying capacity of the composite shows an opposite tendency with increasing fiber volume fraction. However, it should be noted that the composite with the lowest fiber content corresponding to $d_s = 4$ mm behaves similarly to the monolithic $MgAl_2O_4$ that fails catastrophically and does not show fail-safe behavior. On the contrary, the composites with the higher fiber volume fractions ($d_s = 2$ and 1 mm) had a load carrying capacity after matrix cracking. This evidence points out that there is a critical fiber volume fraction or fiber to fiber spacing of the composite that defines the condition at which a fail-safe mechanism can be introduced into the composite due to the load carrying capacity of the intact fibers.

4. Concluding remarks

A unidirectionally aligned SiC fiber preform was incorporated into a $MgAl_2O_4$ matrix with a wide fiber to fiber spacing in order to allow light transmission through the fabricated optomechanical composite. The light transmittance of the $MgAl_2O_4$ decreases with the incorporation of fibers, however it does not diminish totally, and even for the highest fiber volume fraction the light transmittance of the composite changes between 25 and 50% in the visible wavelength region.

Summarizing the results, it is clear that the fracture toughness, K_{Ic}, of the fabricated composites is nearly the same as that of the monolithic matrix, however, a fail-safe mechanism is introduced into the matrix by the incorporation of fibers. Besides the improved mechanical character of the matrix material, its light transmittance is preserved after the incorporation of the fibers. Increasing the fiber volume fraction improves fail-safe capacity whereas the light transmitting capacity shows the opposite tendency. However, it is possible to design an optomechanical composite in which an optimum light transmission and mechanical property pair can be obtained according to the requirements of the desired application.

References

1. R. J. BRATTON, *J. Amer. Ceram. Soc.* **57** (1974) 283.
2. D. W. ROY, in "SPIE Vol. 297: Emerging Optical Materials" (1981) p. 13.
3. C.-T. WANG, L.-S. LIN and S.-J. YANG, *J. Amer. Ceram. Soc.* **75** (1992) 2240.
4. C.-J. TING and H.-Y. LU, *Acta Mater.* **47** (1999) 817.
5. C.-J. TING and H.-Y. LU, *Acta Mater.* **47** (1999) 831.
6. J. J. SWAB, J. C. LASALVIA, G. A. GILDE, P. J. PATEL and M. J. MOTYKA, *Ceram. Eng. Sci. Proc.* **20** (1999) 79.
7. P. HING, *J. Mater. Sci.* **11** (1976) 1919.
8. P. KANGUTKAR, T. CHANG, Y. KAGAWA, M. J. KOCZAK, H. MINAKUCHI and K. KANAMARU, *Ceram. Eng. Sci. Proc.* **14** (1993) 963.
9. Y. KAGAWA, H. IBA, M. TANAKA, H. SATO and T. CHANG, *Acta Mater.* **46** (1998) 265.
10. T. NAGANUMA and Y. KAGAWA, *ibid.* **47** (1999) 4321.
11. J. R. OLSON, D. E. DAY and J. O. STOFFER, *J. Comp. Mater.* **26** (1992) 1181.
12. H. IBA and Y. KAGAWA, in "Composites'95: Proc. Japan-U. S. CCM-VII" (1995) p. 473.
13. H. IBA, T. CHANG and Y. KAGAWA, *J. Amer. Ceram. Soc.* **79** (1996) 881.
14. *Idem.*, *Ceram. Eng. Sci. Proc.* **18** (1997) 787.
15. H. IBA and Y. KAGAWA, *ibid.* **18** (1997) 281.
16. H. IBA, T. NAGANUMA, K. MATSUMURA and Y. KAGAWA, *J. Mater. Sci.* **34** (1999) 5701.
17. A. F. DERICIOGLU and Y. KAGAWA, unpublished data.
18. S. GUO and Y. KAGAWA, *Phil. Mag.* A **80** (2000) 389.
19. K. HONDA and Y. KAGAWA, *Acta Mater.* **44** (1996) 3267.
20. S. Q. GUO, Y. KAGAWA, Y. TANAKA and C. MASUDA, *ibid.* **46** (1998) 4941.
21. D. W. ROY and J. L. HASTERT, *Ceram. Eng. Sci. Proc.* **4** (1983) 502.
22. H. TADA, in "The Stress Analysis of Cracks Handbook" (Paris Productions, St. Louis, USA, 1985) p. 2.19.
23. K. J. KURZYDLOWSKI and B. RALPH, in "The Quantitative Description of the Microstructure of Materials" (CRC Press, Boca Raton, FL, USA, 1995) p. 275.
24. A. F. DERICIOGLU and Y. KAGAWA, *Mater. Sci. Eng. A*, submitted.
25. National Bureau Standards (U. S.) Monogr. 25 (1971) p. 9 25.
26. M. BAAS (Ed.), in "Handbook of Optics Vol. II" (McGraw-Hill, New York, USA, 1995) p. 33.19.
27. Y. KAGAWA, *Mater. Trans. JIM* **35** (1994) 363.
28. Y. KAGAWA and K. SEKINE, *Mater. Sci. Eng.* **A221** (1996) 163.
29. B. BUDIANSKY, J. W. HUTCHINSON and A. G. EVANS, *J. Mech. Phys. Solids* **34** (1986) 167.

Received 28 March
and accepted 16 October 2001